International Journal of Earth Sciences Knowledge and Applications
journal homepage: http://www.ijeska.com/index.php/ijeska
e-ISSN: 2687-5993

Research Article
https://doi.org/10.5281/zenodo.19944120

Time-lapse Geological Assessment of Groundwater; A Case Study of Oghara Farmlands, Delta State, Nigeria

Ozobeme Azubike Anslem[1], Osisanya Olajuwon Wasiu[2]*, Airen Osariere John[1], Ibitoye Taiwo Abel[3], Saleh A. Saleh[3]

[1]*Department of Physics, University of Benin, Benin City, Edo State, Nigeria*
[2]*Department of Applied Geophysics, College of Science, Federal University of Petroleum Resources, Effurun, Delta State, Nigeria*
[3]*Department of Petroleum Engineering and Geosciences, Petroleum Training Institute, Effurun, Delta State, Nigeria*

INFORMATION

Article history
Received 27 January 2026
Accepted 22 April 2026
Published 30 April 2026

Contact
*Osisanya Olajuwon Wasiu
wasiu.osisanya@uniben.edu (OOW)
https://orcid.org/0000-0001-7280-9771

How cite
Anslem, O.A., Wasiu, O.O., John, A.O., 2026. Time-lapse Geological Assessment of Groundwater; A Case Study of Oghara Farmlands, Delta State, Nigeria. *International Journal of Earth Sciences Knowledge and Applications* 8 (1), 168-177. https://doi.org/10.5281/zenodo.19944120.

Abstract
The use of mineral fertilizers and nutrients is widely adopted in conventional agricultural practices, playing an essential role in maintaining optimal crop yields and improving overall quality. To aid farmers in effective fertilization and crop management strategies, non-invasive geophysical techniques can offer insights into the nutrient distribution within the soil. This study deemed it imperative to assess the physicochemical parameters and heavy metals (HM) present in the groundwater of the study area. A total of three groundwater samples and five soil samples were collected and tested for different heavy metals (HM) checked included iron (Fe), chromium (Cr), lead (Pb), copper (Cu), zinc (Zn), nickel (Ni), manganese (Mn), and cadmium (Cd). Recently, electrical resistivity tomography (ERT) has been used in local studies to measure changes in soil properties. Unfortunately, the signals we measure from the ground are mixed up because of changes in the soil both sideways and up and down, making it hard to figure out what each change is contributing. The analysis of groundwater revealed that, with the exception of a few parameters, groundwater samples fell below the WHO permissible limit. The soil's porosity, permeability, and the surrounding topography influence the migration rate. The rates of migration vary between the first and second locations. It has been found that if the vertical migration rate in the dry sand layer (which is about 13.7 meters thick based on drilling data) stays the same, the fertilizer contaminant will take about 0.5 years to reach the wet sandy layer below it in the first location, while in the second location, it will take around 1 year. Detailed calculations to determine the arrival time at the sandy layer have been conducted. Ultimately, it is imperative for the government to guarantee the installation of water purification plants during the process of borehole drilling, as this will help further decrease the existing salinity levels in the groundwater.

Keywords
Baboa de Kole, Alluvial sediments, Geochemistry, Greenstone belt, Tectonic setting

1. Introduction

In conventional agriculture, the application of mineral fertilizers and nutrients is a standard practice essential for achieving optimal yields and high-quality crops. Among these, nitrogen stands out as the most frequently utilized fertilizer; however, its excessive use can result in negative consequences for the environment. To aid farmers in effective fertilization and crop management, non-invasive geophysical techniques can offer insights into the spatial and temporal nutrient distribution within the soil. Agriculture is recognized as a significant contributor to water pollution; however, its geographical characteristics make it particularly challenging

to eliminate this issue (Eyankware et al., 2020a; Eyankware and Obasi, 2021). In the study area, the primary agricultural establishment is the palm oil plantation. The prevalence of groundwater pollution, attributed to intensive agricultural activities, stems from the extensive use of fertilizers in farming practices. Eyankware et al. (2022) have documented the effects of these practices on groundwater contamination. Across various regions of the world, there is a significant reliance on chemical fertilizers (Yang et al., 2006) to boost agricultural productivity. This applies to palm oil plantations as well, where fertilization occurs bi-monthly with fertilizers containing diverse chemical compositions (as noted in a personal discussion with the farming supervisor). At the start of the year, a total of 400 kg of urea containing 60% nitrogen is applied to a two-hectare palm oil plantation. Following this application, after a span of two months, a supplementary fertilizer comprising 15% nitrogen, 30% phosphorus, and 55% potassium (NPK) is utilized to enhance palm production further. This fertilization cycle is repeated in the middle of the year and persists until the year concludes. Overall, a minimum of 800 kg of urea is utilized annually for fertilizing palm trees across the two-hectare area. The leaching of contaminants, particularly nitrates, from agricultural soils has been extensively researched (Aghamelu, et al., 2025; Eyankware et al., 2020; Eyankware et al., 2022). Human activities, such as applying chemical fertilizers in agricultural practices, contribute to nitrate emissions that infiltrate groundwater (Mahvi et al., 2005; Atafare et al., 2010). Research by Islami et al. (2010b) in Kelantan looked into how nitrates contaminate shallow aquifers using a mix of methods, including geoelectrical, hydrogeochemical, and soil property analysis.

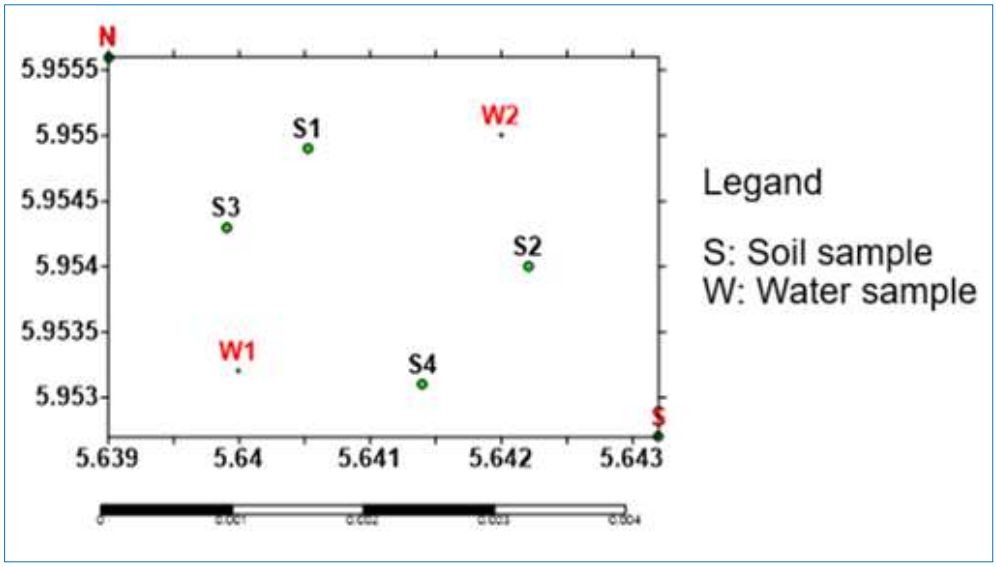

Fig. 1. Base map of the study area

Their findings indicated that areas characterized by intense fertilization activities exhibited comparatively higher nitrate concentrations. Furthermore, Islami (2010a) noted that the geo-electrical resistivity measurements at the surface level in fertilized regions were significantly lower than those in non-fertilized counterparts. When hazardous and harmful substances seep into the earth's subsurface, they contaminate groundwater aquifers, endangering the quality and safety of the water that is eventually stored beneath the surface and made available for human consumption and possibly all other areas of human activity that require water. This phenomenon is known as groundwater pollution (GWP).

Additionally, Ogwah, et al. (2020) pointed out that leftover nitrate and chloride from long-term urea use affect the geoelectrical resistivity measurements in those areas. Obire et al. (2008) also demonstrated that the application of fertilizers adversely affects groundwater quality. Alongside subsurface investigations, several groundbreaking studies utilizing the geoelectrical resistivity imaging technique have been conducted by Barker (1981), Akisnseye et al. (2023), Eyankware and Aleke (2021). The effectiveness of this technique in addressing various geo-environmental issues has been demonstrated through numerous case studies by Esi et al. (2025) and Umuayah and Eyankware (2020).

Nevertheless, there has been no research focused on the use of geoelectrical resistivity imaging for monitoring chemical fertilizers in agricultural settings characterized by specific soil conditions. Furthermore, it is uncommon for geoelectrical imaging surveys to be paid with laboratory analyses of soil water samples collected from the study site, which would enhance the interpretation of field data.

This paper mainly aims to observe how the amounts of chemical fertilizers change over time in the area just below the surface, using methods like geoelectrical resistivity and hydrogeochemical measurements, along with studying soil properties. Additionally, the relationship between fertilizer concentrations in pore soil and geoelectrical resistivity readings was examined, alongside an exploration of nitrate leaching and its dynamics within the sandy soils vadose zone. Monitoring chemical fertilizers in agricultural regions is crucial, given that the primary water supply in these areas is derived from shallow groundwater accessed through conventional wells.

2. Location, Accessibility, Climate and Topography

Oghara, in Delta State (Fig. 1), Nigeria, is characterized by a tropical climate that encompasses two prominent seasons: the dry season and the rainy season. Oghara is characterized by consistently high levels of rainfall, averaging approximately 266.5 cm annually, along with a mean temperature ranging from 24°C (75.2°F) to 27°C (80.4°F) throughout the year. The region experiences two primary seasons: the dry season and the rainy season. The dry season spans from November to February, while the principal rainy season lasts from February to October. July sees the heaviest rainfall, and no month is entirely devoid of rain; January typically receives up to 2.5 cm of precipitation (Aweto and Igben, 2003). The 'harmattan,' which brings cool, dry, and dusty conditions, marks the weather from December to February. Furthermore, the diurnal temperature variation is minimal, with seasonal temperature fluctuations of approximately 25°C (82°F) during the rainy season and 28°C (82°F) in the dry season. The relative humidity in the area ranges from 60 to90 percent (Udo, 1970).

3. Geology of the Study Area/Hydrogeology

The local geological area exhibits three primary depositional (sedimentary) environments: marine, mixed, and continental. Utilizing the classification of sedimentary environments, the sedimentary sequence is characterized by three distinct rock formations: Benin, Agbada, and Akata. In the oil-producing communities of the Niger Delta, the source and seal rocks comprise the marine/deltaic, plastic, and over-pressured shales found within the Akata and Agbada formations. The geological composition of the study area reveals an array of materials, including clay, sand, pebbles, sandstone, gravel, shales, mangrove swamps, lignite, and alluvium.The hydrogeological characteristics of the research area are defined by a multifaceted aquifer system that exhibits diverse groundwater quality and varying degrees of vulnerability. Investigations conducted within this region have primarily aimed at elucidating aspects of groundwater quality, the direction of flow, and the elements that influence the vulnerability of the aquifers (Oseji et al., 2020).

4. Methodology

4.1. Two-dimensional (2D) Resistivity Imaging

The 2D resistivity survey was executed with the use of the PASI Terrameter. Data measurements were taken in sequences at intervals of 10 m, 20 m, 30 m, 40 m, 50 m, and 60 m, employing four (4) electrodes across all traverses, each covering a length of 200 m. The apparent resistivity values for each traverse were organized into a format compatible with the RES2DINV inversion software. Since the surveyed region was relatively flat, elevation corrections were omitted from the measurements. The inversion of the 2D data was performed using the RES2DINV code (Loke and Barker 1996a). For the forward modeling subroutine that computes apparent resistivity values, a grid configuration of 4 nodes per unit electrode along with a normal mesh was employed. The initial and minimum damping factors set for the inversion were 0.225 and 0.05, respectively, contrasting with the default values of 0.160 and 0.015. To account for the exponential decrease in resistivity resolution with depth, the damping factor was permitted to increase by a factor of 1.05 as depth increased. This optimization of the damping factor aimed to considerably decrease the number of iterations needed for convergence, although it resulted in an increase in the time required for each iteration. The complete set of 2D lines, consisting of 10 traverses for both the Erhoike Community and Okpare Community, was integrated to create a unified 3D data set. This integration involved converting the recorded 2D data (apparent resistivity values) into a 3D format compatible with the RES3DINV software (Loke and Barker 1996b) through the utilization of the RES2DINV computer program. To achieve this, the coordinates, line orientations, quantity of electrodes, electrode spacing, and data levels for each of the 2D traverses were employed to compile the apparent resistivity values, assisted by an input text file that the computer code could interpret. The gathered 3D data sets were processed using the RES3DINV software, which automatically generates a 3D model representing the distribution of resistivity based on apparent resistivity measurements acquired from a 3D resistivity imaging survey (Li and Oldenburg 1994; White et al. 2001). For optimal results, the electrodes utilized in such surveys are typically organized in square grids. The inversion technique implemented in the RES3DINV program relies on the smoothness constrained least-squares approach (de Groot-Hedlin and Constable 1990; Sasaki 1992), similar to the method used in RES2DINV for two-dimensional inversions, although a robust inversion can also be performed. This program provides users the flexibility to modify the damping factor and flatness filters within the aforementioned equation to align with the specifics of the data set undergoing inversion. An initial damping factor of 0.215 was employed to invert the assembled 3D apparent resistivity dataset. Following each iteration, the inversion subroutine typically lowered the damping factor applied; a minimum threshold (set at one-tenth of the initial damping factor) was established to ensure the stability of the inversion process. The optimization of the damping factor aimed to minimize the number of iterations needed for the program to achieve convergence by identifying the ideal damping factor that results in the smallest RMS error; however, this optimization consequently lengthens the duration of each iteration. To ascertain the 3D distribution of the model resistivity values based on the apparent resistivity values, the subsurface was divided into several small square blocks. The program established the thickness of the first layer according to the maximum depth of the array's investigation, which was then increased by 1.15 (15%) for the subsequent layers. Finite difference grids consisting of three nodes between neighboring electrodes were employed. A homogeneous earth model served as the initial model for the conducted inversion.

4.2. Groundwater Samples Collection

Water samples from three (3) designated sampling points within the study area were collected. Two (2) of these samples were taken from the impacted zone, while one (1) sample was sourced from a control site situated away from the affected region. Each sample was contained in a one-liter clean plastic bottle and securely sealed. The locations of Well (W1) at PRESCO farmland and Well (W2) at UGBEKUN farmland were recorded utilizing a Global Positioning

System (GPS). Furthermore, a sample was also obtained from a borehole that extends 45 meters deep across the northern, northwestern, and southwestern parts of the area, as depicted in Fig. ****. The sole physical characteristic evaluated in the field was the water's color. The collected samples were directly forwarded to the laboratory for analysis without preservation. Prior to conducting the analysis, the water samples were filtered to remove any suspended particles.

4.3. Soil Sampling

Soil samples were obtained from five (5) distinct sites within the two specified study areas using a soil auger. A steel auger was utilized to extract soil samples from depths of 0 to 15 cm, which were then placed into clear plastic bags for storage. Upon arrival at the laboratory, these samples were air-dried over several days by spreading them on transparent plastic sheets laid out on a workbench. Sampling occurred at varying depths of 0 to 10 cm, 10 to 25 cm, and 25 to 30 cm, respectively. The surface soil was removed to a depth of 15 cm, followed by the extraction of the subsurface soil; this method was uniformly applied to all additional sampling sites. A mechanical shaker was utilized to thoroughly mix the flasks for at least 30 minutes. Subsequently, the resultant materials were filtered through ashless Whatman filter paper 40 and gathered into 100 cm^3 plastic containers.

The control samples underwent initial analysis to determine background target analytes before being spiked with specified concentrations of heavy metals. Following this, a comprehensive extraction procedure was performed to assess the recovery rates. The percent recoveries were calculated by comparing the initial baseline concentrations with those of the spiked samples. For the purpose of spiking the samples with cadmium, cadmium nitrate was prepared as a versatile reagent, ensuring a minimum purity of 99 percent. cadmium nitrate was prepared as a versatile reagent, ensuring a minimum purity of 99 percent. To create solutions for spiking samples with lead, copper, and zinc, analytical-grade lead nitrate, along with analytical-grade granules of copper and zinc, were employed. A reagent blank was prepared for each metal and underwent the full procedural protocol before being utilized for sample analysis. Calibration curves were generated using analytical-grade metals and their respective metal salts.

The concentrations of cadmium, copper, lead, and zinc were assessed using a Varian Techtron AA6 atomic absorption spectrophotometer, paired with the appropriate metallic hollow cathode lamps. Acetylene gas functioned as the fuel source, complemented by air as the supporting medium. An oxidizing flame was consistently applied throughout the process. The concentrations of the four metals were obtained through calibration curves. For instrument calibration, a reagent blank was introduced. Following this, standard solutions were aspirated, and extracts from soil samples were subsequently analyzed.

5. Results and Discussion

5.1. Heavy Metal in Groundwater within the Study Area

5.1.1. Iron (Fe)

The concentration of Fe for this study ranges from 0.02 to 0.14 mg/L, with an average value of 0.07 mg/L as shown in Table 1, and Fig. 2. The allowable threshold for lead in potable water is established at 0.01 mg/L (equivalent to10 µg/L). This maximum concentration is endorsed by the WHO as well as various other health institutions. The presence of iron in drinking water may originate from both natural phenomena and anthropogenic influences. Naturally, iron exists within the earth's crust and can leach into water as it traverses through soil and rock formations (Eyankware, et al., 2019). Furthermore, iron pipes, particularly those exhibiting signs of corrosion, may also release iron into the water supply. Deduction from Fig. 2, showed that the concentration of Fe for this study is above the recommended permissible limit. Eyankware, et al. (2023) were of the view that increase in concentration of Fe may originate from the degradation of iron or steel pipes, as well as other elements within the plumbing system, particularly when the water's acidity, indicated by a pH level, falls below 6.5.

Table 1. Results of physicochemical/heavy metal in groundwater at Presco Low Land and Upland water samples

Parameters	Fe (mg/ L)	Cr (mg/ L)	Pb (mg/ L)	Cu (mg/ L)	Zn (mg/ L)	Ni (mg/ L)	Mn (mg/ L)	Cd (mg/ L)
Sample 1	0.06	0.008	ND	0.02	0.04	<0.005	0.013	ND
Sample 2	0.14	0.021	<0.005	0.05	0.08	<0.005	0.022	ND
Control	0.02	<0.005	ND	0.011	0.014	ND	ND	ND
min.	0.02	0.008	0	0.011	0.014	0	0.013	0
max.	0.14	0.021	0	0.05	0.08	0	0.022	0
aver.	0.07	0.01	0	0.03	0.05	0	0.02	0

5.1.2. Chromium (Cr)

Cr present in drinking water can originate from both natural and anthropogenic sources (Mahapatra et al., 2020). Natural origins encompass processes such as weathering and erosion of rocks and soils, whereas anthropogenic contributions primarily stem from industrial discharges, including those from steel and pulp mills, metal plating facilities, and various other industrial activities. The concentration of Cr for this study ranges from 0.008 to 0.021 mg/L, with an average value of 0.01 mg/L as shown in Table 1, and Fig. 3. The acceptable threshold for total Chromium (Cr) concentration in drinking water is set at 0.05 mg/L, equivalent to 50 µg/L. The permissible limit of Chromium (Cr) is far below the threshold limit. Based on that groundwater is considered safe for drinking.

5.1.3. Lead (Pb)

The presence of lead in drinking water chiefly arises from the corrosion of plumbing materials that contain lead, such as pipes, faucets, and solder used in buildings and water systems (Eyankware, et al., 2022a). Additionally, the leaching of lead into the water may also result from parts of hand pumps or

other substances that include lead or lead-stabilized PVC. The concentration of Pb fell below the permissible limit see Table 1. According to the World Health Organization (WHO) and numerous other entities, the acceptable threshold for lead concentration in drinking water is set at 0.01 mg/L, equivalent to10 µg/L.

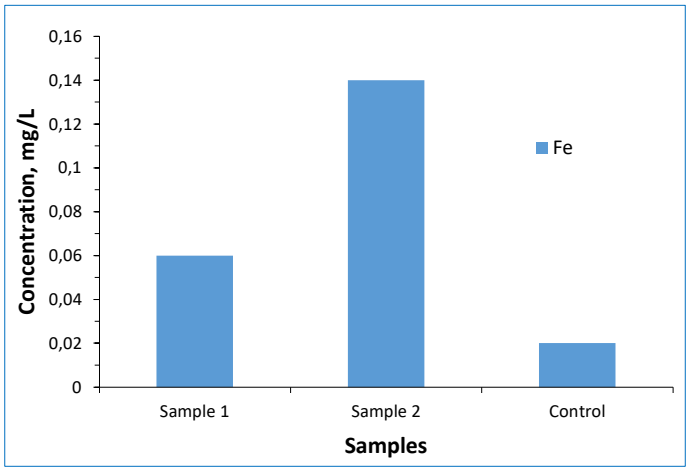

Fig. 2. Plot of Fe against sampling points

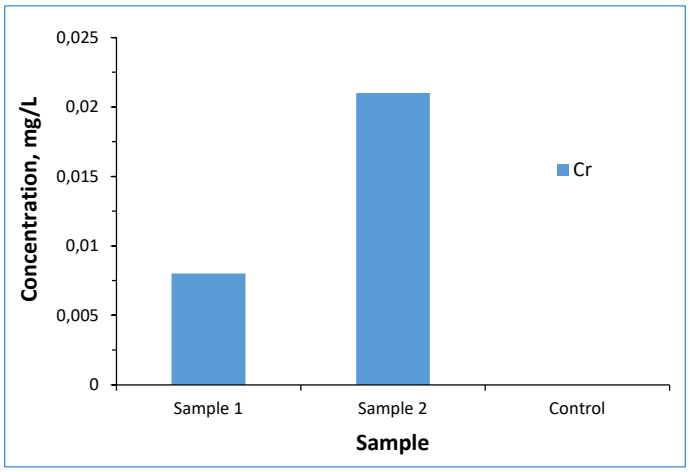

Fig. 3. Plot of Cr against sampling points

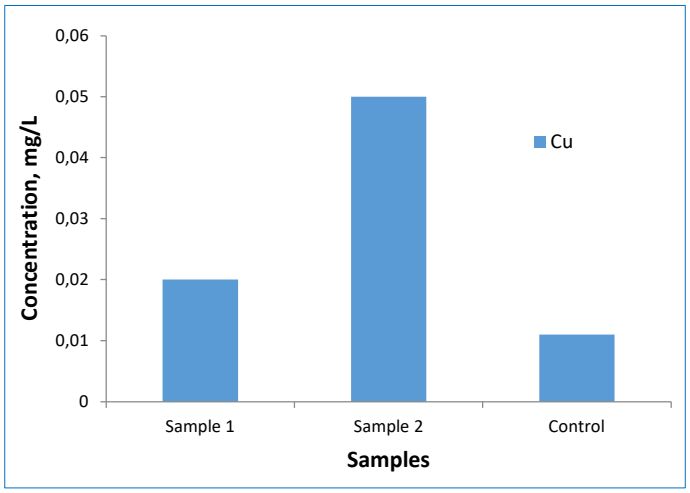

Fig. 4. Plot of Cu against sampling points

5.1.4. Copper (Cu)

The main contributor of Cu in drinking water is the leaching process from copper pipes and fittings within plumbing infrastructures (Eyankware, et al. 2020). This leaching takes place when water interacts with copper components, especially during prolonged periods of stagnation. Additionally, copper may infiltrate the water supply via industrial effluents, wastewater from mining activities, and the natural erosion of rocks containing copper. The concentration of Cu for this study ranges from 0.011 to 0.05 mg/L, an average value of 0.03 mg/L as shown in Table 1, and Fig. 4. The concentration of Cu is below the permissible limit of 2 mg/L recommended by WHO (2011)

5.1.5. Zinc (Zn)

Zn may find its way into drinking water via both natural sources, such as minerals eroded from rocks and soil, and anthropogenic activities, including mining, steel manufacturing, and the utilization of galvanized pipes (Eyankware and Effam, 2019). Furthermore, the introduction of zinc compounds to water is often employed to prevent corrosion, while the deterioration of galvanized pipes or metal fixtures can further elevate zinc concentrations. The concentration of Zn for this study ranges from 0.014 to 0.08 mg/L, with an average value of 0.05 mg/L as shown in Table 1, and Fig. 5. According to the EPA, the acceptable concentration of zinc in drinking water is typically regarded as 5.0 mg/L, equivalent to 5 ppm.

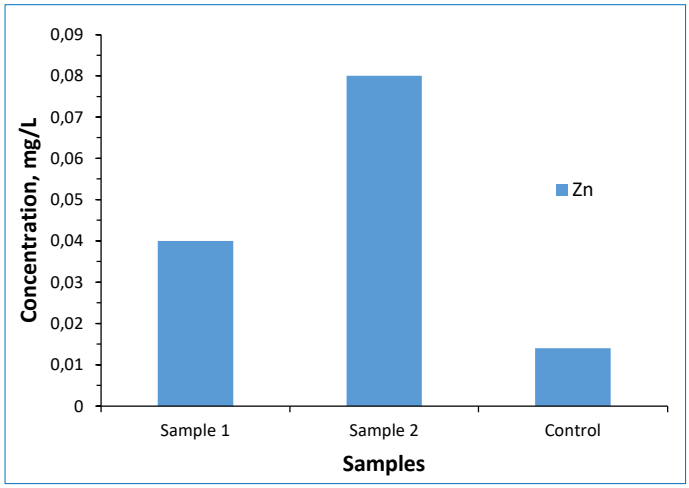

Fig. 5. Plot of Zn against sampling points

5.1.6. Nickel (Ni)

For this study the concentration of Ni is zero, the main source of nickel in drinking water is the leaching process from metals that are in contact with the water, especially those found in nickel or chromium-plated fixtures and internal plumbing systems (Eyankware, et al., 2020; Eyankware, et al., 2018). Furthermore, nickel may also be present naturally in certain groundwater sources as a result of the dissolution of ore-containing rocks. It is probable that no definitive threshold exists for nickel (Ni) in groundwater. According to the WHO (2019), toxicity data pertaining to water-soluble nickel salts proves to be the most relevant in assessing the health risks associated with nickel exposure through drinking water.

Following acute exposure to nickel, individuals may experience gastrointestinal and neurological symptoms, and sensitization to nickel can arise via dermal contact or inhalation. From Table 1, the value of Ni was below zero.

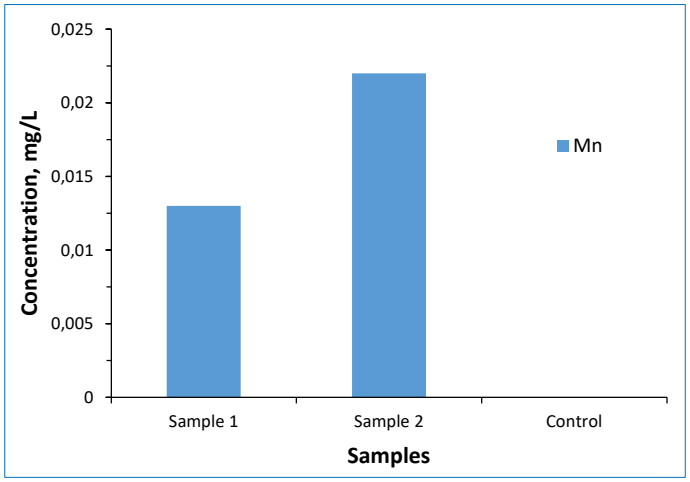

Fig. 6. Plot of Mn against sampling points

5.1.7. Manganese (Mn)

Mn present in drinking water may originate from both natural processes and anthropogenic actions. In nature, manganese is released from minerals found in soil and rock as water filters through these materials, subsequently infiltrating aquifers. Additionally, human endeavors such as mining operations, industrial waste discharges, and leaching from landfills can introduce manganese into water supplies. The concentration of Mn ranges from 0.013 to 0.022 mg/L, with an average value of 0.02 mg/L (Table 1 and Fig. 6).

5.1.8. Cadmium (Cd)

The presence of cadmium in drinking water can be attributed to both natural and anthropogenic sources. On the natural side, cadmium may leach from soils and rocks, whereas human-related activities such as industrial operations, mining activities, and the incorporation of cadmium in numerous products play a significant role in its introduction. The occurrence of Cd was not found in groundwater within the study area (Table 1).

5.2. Discussion on Time Lapse

5.2.1. Time Lapse of Presco Upland

Comprehensive analyses of the soil and water indicated that both sites are influenced by a plume of fertilizer contaminants. The leachate plumes from fertilizers were identified in the initial site (Presco lowland), and a time-lapse study was subsequently conducted to verify the findings from the 2023 ERT survey. The resistivity measurements obtained during the 2024 survey across several lines ranged from 109 Ωm to 2862 Ωm, aligning with the interpretations made in 2023. Furthermore, the time-lapse study conducted at the first site (Presco lowland) to observe the movement of contaminant plumes demonstrated that the highest rate of vertical contaminant migration within the subsurface reached 216.7 cm/month, while the horizontal migration rate was recorded at 750.0 cm/month. A time-lapse investigation of the second site (Presco upland) conducted to observe the movement of contaminant plumes reveals that the highest rate of vertical contaminant migration within the subsurface at this location is 122.5 cm/month, whereas the horizontal migration rate reaches 500.0 cm/month. These findings indicate that both study locations remain significantly active at the time of this assessment. Detailed computations of the migration rates can be found in Table 3 and Table 4.

A subsequent ERT survey was carried out precisely one year later, in April 2024, at which point it is likely that the fertilizer contaminant plumes had either been diluted due to the influx of excess infiltrating water or had experienced additional fertilizer leachate, thereby facilitating a more rapid movement both vertically and horizontally. The migration rate is influenced by the soil's porosity and permeability, as well as the surrounding topography. Notably, the rates of migration observed at the first and second locations exhibit distinct differences.

It has been determined that, assuming a constant vertical migration rate within the dry sand layer, averaging approximately 13.7 meters based on borehole drilling data, it would take roughly 0.5 years and 1 year for the fertilizer contaminants plume to reach the saturated sandy layer directly beneath it at the first and second locations, respectively.

Table 2. Result of Time lapse study of the Presco Lowland

Plume Traverse No	Date	Vertical Position (m)	Horizontal Position (m)	Vertical Migration (m)	Horizontal Migration (m)	Vertical Migration Rate (cm/month)	Horizontal Migration Rate (cm/month)
ERT1	6/08/14 11/08/15	2.8 12.8	8.0 30.0	10.0	22.0	83.3	183.3
ERT3	6/08/14 11/08/15	12.8 39.6	90.0 80.0	26.8	10.0	216.7	83.3
ERT6	6/08/14 11/08/15	39.6 18.5	75.0 90.0	21.1	15.0	175.8	125.0
ERT7	6/08/14 11/08/15	24.9 39.6	95.0 40.0	14.7	50.0	122.5	416.7
ERT8	6/08/14 11/08/15	18.5 24.9	120.0 40.0	6.4	80	53.3	666.7
ERT9	6/08/14 11/08/15	19.8 6.38	22.0 100.0	13.4	78.0	111.7	650.0
ERT11	6/08/14 11/08/15	19.8 15.9	80.0 90.0	3.9	10.0	32.5	83.3
ERT13	6/08/14 11/08/15	6.38 19.8	10.0 100.0	13.4	90	111.7	750

Table 3. Result of time lapse study of the Presco Upland

Plume No	Date	Vertical Position (m)	Horizontal Position (m)	Vertical Migration (m)	Horizontal Migration (m)	Vertical Migration Rate (cm/month)	Horizontal Migration Rate (cm/month)
ERT17	5/08/2014 10/08/2015	31.9 39.6	80.0 140.0	7.7	60.0	64.2	500.0
ERT18	5/08/2014 10/08/2015	24.9 39.6	200.0 160.0	14.7	40.0	122.5	333.3
ERT21	5/08/2014 10/08/2015	24.9 39.6	180.0 200.0	14.7	20.0	122.5	166.7

Table 4. Migrating plume arrival time in subsoil in the different locations

Location	Maximum vertical migration rate (m/month)	Surface layer average thickness (m)	Predicted arrival time in the underlying sandy soil (years)
First location (Presco Lowland)	2.167	13.7	0.5
Second Location (Presco Upland)	1.225	13.7	1

Table 5. Result of time lapse study of the Pesco Lowland

Plume traverse no	Date	Vertical position (m)	Horizontal position (m)	Vertical migration (m)	Horizontal migration (m)	Vertical migration rate (cm/month)	Horizontal migration rate (cm/month)
ERT1	6/08/14 11/08/15	2.8 12.8	8.0 30.0	10.0	22.0	83.3	183.3
ERT3	6/08/14 11/08/15	12.8 39.6	90.0 80.0	26.8	10.0	216.7	83.3
ERT6	6/08/14 11/08/15	39.6 18.5	75.0 90.0	21.1	15.0	175.8	125.0
ERT7	6/08/14 11/08/15	24.9 39.6	95.0 40.0	14.7	50.0	122.5	416.7
ERT8	6/08/14 11/08/15	18.5 24.9	120.0 40.0	6.4	80	53.3	666.7
ERT9	6/08/14 11/08/15	19.8 6.38	22.0 100.0	13.4	78.0	111.7	650.0
ERT11	6/08/14 11/08/15	19.8 15.9	80.0 90.0	3.9	10.0	32.5	83.3
ERT13	6/08/14 11/08/15	6.38 19.8	10.0 100.0	13.4	90	111.7	750

Table 6. Result of time lapse study of the Presco Upland

Plume No	Date	Vertical Position (m)	Horizontal Position (m)	Vertical Migration (m)	Horizontal Migration (m)	Vertical Migration Rate (cm/month)	Horizontal Migration Rate (cm/month)
ERT17	5/08/2014 10/08/2015	31.9 39.6	80.0 140.0	7.7	60.0	64.2	500.0
ERT18	5/08/2014 10/08/2015	24.9 39.6	200.0 160.0	14.7	40.0	122.5	333.3
ERT21	5/08/2014 10/08/2015	24.9 39.6	180.0 200.0	14.7	20.0	122.5	166.7

Table 7. Migrating plume arrival time in subsoil in the different locations

Location	Maximum vertical migration rate (m/month)	Surface layer average thickness (m)	Predicted arrival time in the underlying sandy soil (years)
First location (Presco Lowland)	2.167	13.7	0.5
Second Location (Presco Upland)	1.225	13.7	1

The specifics of the calculations regarding the arrival time at the sandy layer are detailed in Table 5. Furthermore, it is evident that the horizontal migration rate surpasses the vertical migration rate, with differences of 133.4 cm/month and 210.8 cm/month observed in the second and third cemetery, respectively.

5.2.2. Time Lapse of Presco Lowland

The fertilizer leachate plumes were in the first location (Presco lowland), a time lapse study in ERT survey. The resistivity recorded for the 2024 survey on some survey lines varied from 109 Ωm to 2862 Ωm. A time lapse study of the first location (Presco lowland) to monitor the migration of contaminants plumes shows that the maximum rate of contaminant migration within the subsurface in the vertical direction in the first location is 216.7 cm/month, while the horizontal migration rate is750.0 cm/month respectively. While a time lapse study of the second location (Presco upland) to monitor the migration of contaminants plumes shows that the maximum rate of contaminant migration within the subsurface in the vertical direction in the second location is 122.5 cm/month, while the horizontal migration

rate is 500.0 cm/month respectively. These results show the status of the study locations: the first and the second location are much still more active as at the time of this survey.

Table 6 and Table 7 give the details of the computation of migration rates. The first ERT survey was conducted in April 2023, and fertilizer contaminant plumes were delineated. The second ERT survey was executed exactly 12 months later, in April 2024, when the fertilizer contaminate plumes must have been diluted with excess infiltrating water or more fertilizer leachate added and so move faster in the vertical and horizontal directions. The rate of migration depends on the porosity and permeability of the soil and topography. The migration rates are distinctive in the first and second location. However, it is revealed that if the vertical migration rate is constant in the dry sand layer (average thickness of about 13.7 m from borehole drilling information), then it will take about 0.5 and 1 years for the fertilizer contaminants plume in the first and second location respectively to arrive at the saturated sandy layer just below it.

Table 7 shows the detail of the computation of arrival time to the sandy layer. Moreso, it is also seen that the rate of migration in the horizontal direction is higher than that in the vertical direction by margins of 133.4 cm/month and 210.8 cm/month and in the second and third cemeteries respectively.

Conclusion

This study carried out assessment of water and soil impacted by application of fertilizer within study area for physico-chemical, and heavy metals concentration. A total of three (3) groundwater samples were carried out within the study area, one ot of the three sample was used as control site. As for soil, a total of four (4) , two (2) each from each sample site. In the study presented, time-lapse geophysical measurement using ERT was used to analyze the impact of fertilization on the measured geophysical signals. Analysis of the groundwater and soil indicated that the groundwater samples fell below the permissible limits set by the WHO, with the exception of a few parameters. The migration rate is influenced by the soil's porosity and permeability as well as the topographical features. Notably, the migration rates differ between the first and second locations. It has been determined that, assuming a consistent vertical migration rate within the dry sand layer (approximately 13.7 m thick based on borehole drilling data), the fertilizer contaminants plume will reach the saturated sandy layer beneath in approximately 0.5 years at the first location and 1 year at the second location. Detailed calculations regarding the arrival time to the sandy layer.

References

Aghamelu, O.P., Eyankware, M.O., Akakuru O.C., 2025. Geochemical characterization and risk implications of groundwater for irrigation and drinking around the agrarian metropolis of southeastern Nigeria. Sustainable Water Resources Management 11 (6), 133.

Abu-Hassanein, Z.S., Benson, C.H., Blotz, L.R., 1996. Electrical resistivity of compacted clays. Journal of Geotechnical Engineering 122, 397-406.

Ahmed, A., Hossain, M.S., Khan, M.S., Greenwood, K., Shishani, A., 2017. Moisture Variation in Expansive Subgrade through Field Instrumentation and Geophysical Testing. In Proceedings of the International Congress and Exhibition "Sustainable Civil Infrastructures: Innovative Infrastructure Geotechnology", Sharm El Sheikh, Egypt, 15–19 July 2017; Springer: Cham, Switzerland, pp. 45-58.

Aizebeokhai, A.P., . 2010. 2D and 3D geoelectrical resistivity imaging: Theory and field design. Scientific Research and Essays 5 (23), 3592-3605.

Akinseye, V.O., Osisanya, W.O., Eyankware. M.O., Korode, I.A., Ibitoye, A.T., 2023. Application of second-order geoelectric indices in determination of groundwater vulnerability in hard rock terrain in SW. Nigeria. Sustainable Water Resources Management 9, 169. https://doi.org/10.1007/s40899-023-00936-w.

Akpoborie, I.A., Aweto, K.E., Ohwoghere-Asuma, O., 2015. Urbanization and major ion hydrogeochemistry of the shallow aquifer at the Effurun-Warri metropolis, Nigeria. Environment and Pollution 4 (1), 37.

de Groot-Hedlin, C., Constable, S., 1990. Occam's Inversion to Generate Smooth, Two-Dimensional Models from Magnetotelluric Data. Geophysics 55, 1613-1624. https://doi.org/10.1190/1.1442813.

Emmanuela, A.A., Wasiu, O.O., Eyankware M.O., 2024. Delineation of groundwater potential using electrical resistivity imaging techniques at Ibule Akure, Southwestern Nigeria. Malaysian Journal of Geosciences 8 (1), 01-09.

Ekwue, E., Bartholomew, J., 2011. Electrical conductivity of some soils in Trinidad as affected by density, water and peat content. Biosystem Engineering 108, 95-103.

Esi, E.O., Orisekpabor O.P., Eyankware, M.O., 2025. Integration of geophysical and radiological assessment of solid waste diposal impact on groundwater and human health in southern Nigeria. Geosystems and Geoenvironment 5 (1), 100425. https://doi.org/10.1016/j.geogeo.2025.100425.

Eyankware. M.O., Nnajieze, V.S., Aleke, C.G., 2018. Geochemical assessment of water quality for irrigation purpose, in abandoned limestone quarry pit at Nkalagu area, Southern Benue Trough Nigeria 77, 66. https://doi.org/10.1007/s12665-018-7232-x.

Eyankware. M.O., Effam, S.C., 2019. A preliminary assessment of hydrogeochemical quality of groundwater around rural communities of abandoned Nkalagu limestone quarry. SE Nigeria. Annals of Chemical Science Research 1 (5), ACSR.000522.2019. https://doi.org/10.31031/ACSR.2019.01.000522.

Eyankware. M.O., Omo-Irabor, O.O., 2019. An integrated approach to groundwater quality assessment in determining factors that influence the geochemistry and origin of sandstone aquifers, Southern Niger Delta Region of Nigeria. Malaysian Journal of Geosciences 3 (2), 23-32. https://doi.org/10.26480/mjg.02.2019.23.32.

Eyankware, M.O., Igwe, E.O., Ulakpa, R.O.E., Ogwah, C., 2020a. Achieving sustainable use and management of water resources for irrigation in Nigeria-Review. Journal of Environmental & Earth Sciences 2 (2), 47-55.

Eyankware. M.O., Ogwah, C., Ulakpa. R.O.E., 2020b. The study of sea water intrusion in coastal aquifer of Niger Delta Region, Nigeria. Middle-East Journal of Scientific Research 28 (4), 369-379.

Eyankware., M.O., Ephraim, B. E., 2021. A comprehensive review of water quality monitoring and assessment in Delta State, Southern Part of Nigeria. Journal of Environmental and Earth Sciences 3 (1), 16-28. https://doi.org/10.30564/jees.v3i1.2900.

Eyankware, M.O., Aleke, G., 2021. Geoelectric investigation to

determine fracture zones and aquifer vulnerability in southern Benue Trough southeastern Nigeria. Arabian Journal of Geosciences 14, 2259. https://doi.org/10.1007/s12517-021-08542-w.

Eyankware. M.O., Obasi, P.N., 2021. A holistic review of heavy metals in water and soil in Ebonyi SE. Nigeria; with emphasis on its effects on human, aquatic organisms and plants. World News of Natural Science 38, 1-19.

Eyankware, M.O., Ogwah, C., Umayah, O.S., 2021. Integrated geophysical and hydrogeochemical characterization and assessment of groundwater vulnerability in Adum West Area of Benue State, Nigeria. Journal of Geophysical Research 65, 6588128. https://doi.org/10.30564/jgr.v3i3.3197.

Eyankware, M.O., Akakuru, C.O., Ulakpa, R.O.E., Eyankware, E.O., 2022a. Hydrogeochemical approach in the assessment of coastal aquifer for domestic, industrial, and agricultural utilities in Port Harcourt urban, southern Nigeria. International Journal of Energy and Water Resources 7, 401-419. https://doi.org/10.1007/s42108-022-00184-2.

Eyankware. M.O., Akakuru, C.O., Eyankware, E.O., 2022b. Hydrogeophysical delineation of aquifer vulnerability in parts of Nkalagu areas of Abakaliki, SE. Nigeria. Sustainable Water Resources Management 8, 39. https://doi.org/10.1007/s40899-022-00603-6.

Eyankware, M.O., Akakuru, O.C., Inoni, O.E., Osisanya, W.O., Ukor, K.P., Umuokoro, G., 2025a. Interpretation of hydrochemical data in selected parts of Warri, Southern Nigeria using health risk assessment and heavy metal index. Discovery Nature 2 (3), 1-34. https://doi.org/10.54905/disssi.v2i3.e6dn3107.

Eyankware, M.O., Mba-Otike, M.N., Odesa, G.E., Chukwusa, F. O., Osisanya, W.O., Eyankware-Ulakpa, R.O., Akakuru, O.C., Komolafe, N.P., 2025b. Saline intrusion in Niger Delta coastal aquifers, drivers, hydrogeological dynamics and mitigation strategies. Discover Geoscience, 3, 150. https://doi.org/10.1007/s44288-025-00264-w.

Eyankware, M.O., Emudiaga, O.E., Ukor, K.P., Okudibie, E.J., 2026. Water bearing unit, not everywhere; Resistivity study of shallow aquifer around Patani Milieu, Niger delta region of Nigeria. Discovery Nature 3 (5), e2dn3159.

Giao, P., Chung, S., Kim, D., Tanaka, H., 2003. Electric imaging and laboratory resistivity testing for geotechnical investigation of Pusan clay deposits. Journal of Applied Geophysics 52, 157-175.

Ghorbani, A., Revil, A., Bonelli, S., Barde-Cabusson, S., Girolami, L., Nicoleau, F., Vaudelet, P., 2024. Occurrence of sand boils landside of a river dike during flooding: A geophysical perspective. Engineering Geology 329, 107403.

Hossain, M.S., Maganti, D., Hossain, J., 2010. Assessment of geo-hazard potential and site investigations using Resistivity Imaging. International Journal of Environmental Technology and Management 13, 116-129. https://doi.org/10.1504/IJETM.2010.034297.

Kalinski, R., Kelly, W., 1993. Estimating water content of soils from electrical resistivity. Geotechnical Testing Journal 16, 323-329.

Islami, N. Taib, S. Yusoff, I. Ghani A.A., 2011. Time lapse chemical fertilizer monitoring in agriculture sandy soil. International Journal of Environmental Science & Technology 8 (4), 765-780.

Islami, N., Irianti, M., Fakhruddin, F., Azhar, A., Nor M., 2020. Application of geoelectrical resistivity method for the assessment of shallow aquifer quality in landfill areas. Environmental Monitoring and Assessment 192 (9), 606.

Jabrane, O., Martínez-Pagán, P., Martínez-Segura, M.A., Alcalá, F.J., El Azzab, D., Vásconez-Maza, M.D., Charroud, M., 2023. Integration of Electrical Resistivity Tomography and Seismic Refraction Tomography to Investigate Subsiding Sinkholes in Karst Areas. Water 15, 2192.

Mahvi, A.H., Nouri, J., Babaei, A.A., Nabizadeh, N., 2005. Agricultural activities impact on groundwater nitrate pollution. International Journal of Environmental Science & Technology 2, 41-47. https://doi.org/10.1007/BF03325856.

Martínez-Pagán, P., Gómez-Ortiz, D., Martín-Crespo, T., Manteca, J., Rosique, M., 2013. The electrical resistivity tomography method in the detection of shallow mining cavities. A case study on the Victoria Cave, Cartagena (SE Spain). Engineering Geology 156, 1-10.

McCarter, W.J., 1984. The electrical resistivity characteristics of compacted clays. Geotechnique 34, 263-267.

Obire, O., Douglas, S.I., Chuku J.I., 2021. Evaluation of the Impact of Anthropogenic Activities on the Microbiological Quality of Azumini Odumanya Stream, Port Harcourt, Nigeria. International Journal of Current Microbiology and Applied Sciences 10 (07), 143-153. https://doi.org/10.20546/ijcmas.2021.1007.017.

Odesa, G.E., Okanigbuan P.N., Eyankware, M.O., NgoziChika, C.S., Oghenetega, E., 2025. Health risk assessm,ent of water resources within the lignite series of Obomkpa and environs, southern Nigeria. Journal of Contaminant Hydrology. https://doi.org/10.1016/j.jconhyd.2025.104665.

Ogwah, C., Eyankware, M.O., 2020. Investigation of Hydrogeochemical processes in groundwater resources located around abandoned Okpara coal mine, Enugu SE. Nigeria. Journal Clean Was 4 (1), 12-16. http://doi.org/10.26480/cleanwas.01.2020.12.16.

Okolo, C.M., Obasi P.N., Akpa, C., Eyankware M.O., Onwe I.M., Edene E.N., Nweke O.M., Ani C.C., Alieze I.V., Omeokachie A.I., Nworie C.D., 2025. Assessment of the lower drainage basin aquifers for domestic, industrial, and agricultural uses in Onitsha commercial area, Southern Nigeria using hydrochemical approach. Environment, Development and Sustainability 2025. https://doi.org/10.1007/s10668-025-06741-z.

Omo-Irabor, O.O., Eyankware. M.O., Ogwah, C., 2018. Integration of hydrogeochemical analytical methods and irrigation parameters in the evaluation of groundwater quality at Ibinta, Southern Benue Trough Nigeria. Journal of Scientific and Industrial Research 2 (1), 38-49.

Onwe, I.M., Eyankware. M.O., Obasi, P.N., Ifeanyichukwu, K.A., 2022. Hydrochemical and statistical approaches in the evaluation of groundwater quality for drinking and irrigation uses around Ezzangbo–Ngbo area, Southeastern Nigeria. Modeling Earth Systems and Environment 9, 413-429. https://doi.org/10.1007/s40808-022-01503-6.

Onwe, I.A. Obasi, Eyankware, M.O., Uchenna, O.L., 2024. An integration of hydrochemical data and stable isotopes in groundwater evaluation in Ngboejogu, Southern Benue Trough, Nigeria. Modeling Earth Systems and Environment 10, 7207-7223. https://doi.org/10.1007/s40808-024-02166-1.

Oseji, O.T., Egbai, J.C., Emuobonuvie, I.A., 2020. Aquifer vulnerability using geophysical and physiochemical methods in parts of Ethiope West Local Government Area of Delta State, Nigeria. Advances 10, 085209. https://doi.org/10.1063/5.0015357.

Osisanya, W.O., Agbalagba, E.O., Ife-, I.O., Agho, O., Eyankware, M.O., Iduseri, O.M., 2025. An in-depth study of heavy metals in soils around selected waste dumpsites in parts of southern Nigeria using heavy metal indices and multivariate statistical

analysis. Global Journal of Pure and Applied Sciences 31, 735-750.

Power, C. Gerhard, J.I. Karaoulis, M., Tsourlos, P., Giannopoulos, A., 2014. Evaluating four-dimensional time-lapse electrical resistivity tomography for monitoring DNAPL source zone remediation. Journal of Contaminant Hydrology 162-163, 27-46. https://doi.org/10.1016/j.jconhyd.2014.04.004.

Samouëlian, A., Cousin, I., Tabbagh, A., Bruand, A., Richard, G., 2005. Electrical Resistivity Survey in Soil Science: A Review. Soil and Tillage Research 83, 173-193. https://doi.org/10.1016/j.still.2004.10.004.

Sasaki, Y., 1992. Resolution of Resistivity Tomography Inferred from Numerical Simulation. Geophysical Prospecting 40, 453-464. https://doi.org/10.1111/j.1365-2478.1992.tb00536.x.

Sehgal, M., Garg, A., Suresh, R., Dagar, P.,(2012. HM contamination in the Delhi segment of Yamuna basin. Environmental Monitoring Assessment 184, 1181-1196. https://doi.org/10.1007/s10661-011-2031-9.

Singh, V.K., Singh, K.P., Mohan, D., 2005. Status of heavy metals in water and bed sediments of River Gomti—a tributary of the Ganga River, India. Environmental Monitoring Assessment 105, 43-67.

Short, K.C., Stauble, A.J., 1967. Outline of geology of Niger Delta. American Association of Petroleum Geologists Bulletin 51, 761-779.

Tabbagh, A., Dabas, M., Hesse, A., Panissod, C., 2000. Soil resistivity: A non-invasive tool to map soil structure horizonation. Geoderma 97, 393-404.

Udo, R.K., 1970. Geographical Regions of Nigeria. Heinemann Educational Books, London.

Umayah, O.S., Eyankware, M.O., 2022. Aquifer evaluation in southern parts of Nigeria fromgeo-electrical derived parameters. World News of Natural Science 42, 28-43.

WHO, 2011. Guidelines for drinking water quality, 4th edn. NLM classifcation: WA 675, World Health Organization, Geneva, Switzerland, pp 307-433.